Article

Discovery Medicine 2026; 38(204): 155–170
https://doi.org/10.24976/Discov.Med.202638204.13

RBP3-Loaded Exosomes Suppress Pathological Retinal Angiogenesis Through Disrupting Endothelial DNA Replication

Huimin Zhu[1,†], Min Zhao[1,†], Wen Zhou[1], Mengzhu Wang[1], Yongxuan Liu[1], Hao Zeng[1], Mai Peng[1], Zheng Nie[1], Jianjun Jia[1], Chengyue Ding[1], Xinwei Wang[1], Hongyuan Song[1,*], Wei Shen[1,*]

[1]Department of Ophthalmology, Shanghai Changhai Hospital (The First Affiliated Hospital of Naval Medical University), 200433 Shanghai, China
*Correspondence: hongyuansong@hotmail.com (Hongyuan Song); shenwei@smmu.edu.cn (Wei Shen)
[†]These authors contributed equally.
Submitted: 18 September 2025 Revised: 26 November 2025 Accepted: 12 December 2025 Published: 20 January 2026

Background: The damage caused by pathological angiogenesis to visual function is grievous. Retinol-binding protein 3 (RBP3) demonstrates an inverse relationship with diabetic retinopathy (DR) progress and suppresses pathological retinal angiogenesis under hyperglycemic conditions. However, the impact of externally administered RBP3 in such pathological retinal angiogenesis remains undefined. This research explores how intravitreally delivered RBP3-loaded exosomes (RBP3-Exo) curtail abnormal retinal vessel growth.

Methods: We generated RBP3-Exo with safety and good biocompatibility using plasmid transfection technology. The anti-angiogenic effect of RBP3-Exo was evaluated *in vitro* through cell proliferation, sprouting assays, and other experiments. Using an oxygen-induced retinopathy (OIR) model, we administered exosomes intravitreally and conducted subsequent staining assays to evaluate angiogenic activity *in vivo*. RNA-seq was conducted, which revealed that its main target pathway is the DNA replication pathway, and this was verified by Real-time quantitative polymerase chain reaction (qPCR) and Western blot.

Results: Results indicate that RBP3-loaded exosomes markedly restrain endothelial cell proliferation and sprouting in laboratory settings. In OIR mice, they also diminish both avascular retinal zones and pathological neovascular tuft formation. Mechanistically, RBP3-loaded exosomes may achieve these effects by interfering with DNA replication processes.

Conclusion: In conclusion, RBP3-Exo potently suppress pathological retinal angiogenesis, positioning them as a compelling therapeutic candidate for ocular neovascular diseases.

Keywords: pathological retinal angiogenesis; OIR model; DNA replication; RBP3; exosomes

Introduction

Pathological retinal angiogenesis, characterized by intraretinal hemorrhage, exudation, and proliferative vasculopathy, confers a significant risk of blindness and profoundly impairs quality of life [1]. As a dynamic biological cascade orchestrated by vascular endothelial cells, angiogenesis in neovascular eye diseases is hallmarked by localized hypoxia-ischemia and aberrant neovascular sprouting [2,3]. Whereas physiological angiogenesis maintains tissue homeostasis and facilitates repair, its pathological manifestation exacerbates morbidities in conditions ranging from oncogenesis to rheumatoid arthritis [4]. Disorders of the eye's new blood vessels, such as diabetic retinopathy, retinal vein blockage, arterial blockage and retinopathy of prematurity (ROP), invariably lead to significant visual deficits [5–7]. Current anti-vascular endothelial growth factor (anti-VEGF) monotherapies represent the therapeutic mainstay for neovascular ophthalmopathies; however, clinical translation is hampered by prohibitive costs, requirement for repeated intravitreal administrations, and emerging resistance profiles [8–10]. Conventional interventions, including panretinal photocoagulation and anti-VEGF biologics, further suffer from off-target systemic toxicities arising from non-selective pathway inhibition. Of particular import, pathological retinal angiogenesis in diseases such as diabetic retinopathy and retinopathy of prematurity has spurred investigation into nanomedicine-based strategies, which hold promise to mitigate limitations of traditional therapies—including invasiveness, pharmacoresistance, and systemic side effects—thereby fostering the development of precision anti-angiogenic therapeutics.

Retinol-binding protein 3 (RBP3), secreted by photoreceptors, is crucial in imparting resistance to DR [11–13]. It exerts this protective effect by potently inhibiting the VEGF signaling pathway, a key driver of retinal vascular dysfunction in diabetes [14]. By block-

ing VEGF-mediated responses, RBP3 effectively mitigates hyperglycemia-induced retinal inflammation and vascular lesions, safeguarding the retina from the deleterious effects of prolonged high glucose levels. This mechanism underscores RBP3's importance as a potential endogenous protective factor against DR progression [15].

Exosomes, small membrane-bound vesicles (50–150 nm) secreted by cells, serve as pivotal mediators of intercellular communication [16–18]. Encased within these nanovesicles is a varied array of lipids, RNAs, proteins, and even organelles, facilitating their role in regulating physiological functions through the transfer of bioactive molecules to target cells. Owing to their minimal immune response, robust stability, and high compatibility with biological systems, exosomes have emerged as viable substitutes for cellular therapies, especially in the realms of medication administration and diagnostics [16]. In the context of ocular fundus diseases, exosomes exhibit pleiotropic functions: they may promote pathological angiogenesis in age-related macular degeneration (AMD) by carrying pro-angiogenic factors, while in DR, they are intricately linked to inflammatory responses and vascular damage [19–22]. These dual roles highlight exosomes as both pathogenic mediators and potential therapeutic targets. Concurrently, research into exosome-based drug carriers is gaining traction, leveraging their unique physical properties to enable targeted delivery in retinal disorders [9]. As natural nanocarriers, exosomes combine size-dependent tissue penetration with innate biological functionality, positioning them at the forefront of nanomedicine. Their utility in precision therapy is further underscored by advantages such as reduced systemic toxicity and minimized immune rejection, making them ideal platforms for developing next-generation therapeutics for ocular and systemic diseases [23–26].

Aberrant DNA replication is intrinsically linked to DR and pathological retinal neovascularization. Under hyperglycemic conditions, oxidative stress and advanced glycation end products (AGEs) accumulate, inflicting DNA damage and replication inaccuracies within vascular endothelial cells. This subsequently triggers DNA repair mechanisms or precipitates cellular apoptosis [27]. Concurrently, there is a dysregulated expression of pro-angiogenic mediators, notably VEGF, instigating unchecked endothelial cell proliferation. This drives, pathological retinal angiogenesis, thereby accelerating DR progression, as evidenced in the oxygen-induced retinopathy (OIR) model [28,29]. The roles of RBP3 and exosomes in this cascade are under investigation.

This research shed light on how RBP3-loaded exosomes (RBP3-Exos) plays a crucial role in treating pathological angiogenesis. Initially, HEK293t cells were transfected with the RBP3 gene construct and empty vector control, followed by collection of cell culture supernatants. Isolation of exosomes was achieved via ultracentrifugation, followed by RNA-seq analysis indicating RBP3-Exos' potential inhibitory effects on VEGF-driven signaling and DNA replication pathways. The results reveal that the genetically modified RBP3-Exos hold significant promise for treating pathological angiogenesis, marked by pronounced vascular specificity and low overall toxicity.

Materials and Methods

Cell Cultures

Human Umbilical Vein Endothelial Cells (HUVECs) are a suitable cell type for studying pathological neovascularization in diabetic retinopathy [30]. HUVECs for experimental were sourced from Zishan Biotechnology (Wuhan, China, #STCC12103). HEK293t cells were purchased from Noble Biotechnology (Zhejiang, Chian, #nobcell0005). The cells used in the experiment were identified by short tandem repeat (STR) analysis. The results showed a match rate of $\geq$98% with the standard profile of the cell line, confirming the correct cell identity and the absence of cross-contamination. Meanwhile, mycoplasma detection was performed using the fluorescence staining method, and the cell samples tested negative for mycoplasma, eliminating the interference of mycoplasma contamination on the experimental results. These cells underwent cultivation within a DMEM (YuliBiotech #LD1111-500, Shanghai, China) supplemented 10% FBS (YuliBiotech #S1001-500, Shanghai, China), maintained under hypoxic conditions of 1% O_2 at 37 °C. The culture was sustained until reaching a target confluence of approximately 80%.

Preparation and Characterization of RBP3-Exo

For RBP3-Exos production, HEK293t cells underwent transfection with a plasmid encoding the *RBP3* gene (see **Supplementary Material 1**). The control group in this study is the empty vector group, where cells were transfected with an empty vector plasmid lacking the *RBP3* gene. Approximately 60 hours' transfection, exosomes isolation was performed via established differential centrifugation [31]. Initially, conditioned medium was subjected to centrifugation at 300 g (10 min, 4 °C) for cellular removal. The resulting supernatant was then centrifuged twice at 2000 g (20 min, 4 °C) to eliminate debris. A final ultracentrifugation (Beckman Optima XE-100) step at 100,000 g (120 min, 4 °C) pelleted the exosomes, which were subsequently washed and resuspended with phosphate buffer saline (PBS).

A BCA protein assay kit (Servicebio #G2026, Wuhan, China) was utilized to measure the concentration of exosomes. The transfection efficiency and successful extraction of exosomes were validated through two sequential steps. First, in terms of exosome characterization, transmission electron microscopy (TEM) was employed for morphological observation, while nanoparticle tracking analysis (NTA) was used to determine size distribution, and these analyses collectively confirmed the successful extraction of

exosomes. Second, Western Blot (WB) verification was conducted, and the detection of a specific RBP3 protein band in the exosomes confirmed that the transfected cells secreted exosomes containing RBP3.

The internalization of exosomes by HUVECs was evaluated using DiD-tagged RBP3-Exos. In summary, RBP3-Exos were underwent a 30-minute incubation with DiD (Beyotime #C1039, Shanghai, China) at 37 °C. DiD-labelled RBP3-Exos underwent a 12-hour co-incubation with HUVECs, followed by analysis through confocal microscopy.

Transmission Electron Microscopy (TEM)

For the TEM detection of exosomes, we use the negative staining method. Take 100 µL of the sample, add 2% paraformaldehyde, and fix it at room temperature for 5 minutes. Pipette a small amount of the sample and drop it onto a copper grid. After allowing the sample to adsorb naturally for a moment, absorb the excess liquid with filter paper. Then, add 10 µL of phosphotungstic acid to stain the sample, let it stand for 1 minute, absorb the excess staining solution again, and allow the copper grid to air-dry. Finally, place the dried copper grid under a transmission electron microscope (Hitachi #HT7700, Tokyo, Japan), adjust the magnification (10,000–40,000×), and perform observation and photography.

Nanoparticle Tracking Analysis (NTA)

Take the purified exosome suspension, filter it through a 0.22 µm sterile filter membrane to remove impurities, dilute it with sterile PBS in a gradient manner to a concentration of 1×10^8–5×10^8 particles/mL, and then vortex to mix thoroughly. After preheating the instrument (Particle Metrix #ZetaView PMX120, Meerbusch, North Rhine-Westphalia, Germany) and calibration, pipette 1 mL of the pretreated sample into the sample cell, adjust parameters such as detection duration and shutter speed, start the program to track the Brownian motion of exosomes, and analyze by combining with the Stokes-Einstein equation to generate particle size-related results.

Sprouting Assay

The *in vitro* spheroid sprouting assay was employed to evaluate the angiogenic influence of RBP3-Exos. HUVECs, at a density of 20,000 cells/mL, were resuspended in either control medium or medium supplemented with RBP3-Exos, combined with a methylcellulose solution, and subjected to inverted incubation for 24 h. Following a gentle PBS wash and centrifugation, the resulting spheroids were resuspended in a methylcellulose (Sigma #M0512) solution containing 20% FBS (Yuli-Biotech #S1001-500, Shanghai, China). A Collagen type I (Corning #CLS354236) was prepared by mixing with 10× Medium 199 (Sigma #M0650), and the pH adjustment achieved to neutral using NaOH. This collagen mixture was then combined with methylcellulose solution harboring the spheroids. Aliquots of the spheroid-collagen suspension were transferred to a 24-well plate and simulated for 48 hours within a hypoxia incubator (37 °C, 1% O_2) with 200 µL of DMEM supplemented with either PBS, Exos or RBP3-Exos (50 µg/mL). Subsequent imaging via microscopy enabled the quantification of sprout numbers and total sprouting length utilizing ImageJ software (1.54f, National Institutes of Health, USA).

Cell Proliferation Assay

Assessment of cellular proliferation was conducted via 5-ethynyl-2′-deoxyuridine (EdU) assays. A total of 2000 cells per well were seeded in 96-well plates and exposed to PBS, Exos or RBP3-Exos for 48 hours under hypoxic conditions. Following the supplier's instructions, cells were incubated with EdU (Huilan Biotechnology #RCF041, Shanghai, China) working solution (1:1000 dilution) for 2 h, then fixed using 4% PFA (Servicebio #G1101, Wuhan, China) for 30 min. Glycine (Sinopharm #62011516, China, 2 mg/mL ddH_2O) was subsequently applied for 5 min to wash the cells, which were then rinsed twice with PBS containing Triton X-100 (Servicebio #GC204003, Wuhan, China). Thereafter, an incubation step with Apollo fluorescent azide proceeded for 30 min at ambient temperature, shielded from light, succeeded by three additional washes with PBS containing Triton X-100. 4′,6-Diamidino-2-phenylindole dihydrochloride (DAPI, Invitrogen #D1306) staining followed for 15 min, after which the cells underwent PBS rinsing. Proliferation rates were determined as the ratio of EdU-positive nuclei to DAPI-positive nuclei. Fluorescence microscopy captured the images, and quantification was executed using ImageJ (1.54f, National Institutes of Health, USA).

CCK8 Assay

Cell proliferation was assessed via a CCK8 kit (Yeason #40203ES60, Shanghai, China), conducted in strict adherence to the manufacturer's instructions. Briefly, cells were seeded into 96-well plates at a density of 2×10^3 cells per well in 100 µL of culture medium and allowed to adhere for 24 hours under standard conditions (37 °C). Following this incubation, the cells were exposed to PBS, Exos or RBP3-Exos (50 µg/mL) and maintained for 48 h within a hypoxic environment (1% O_2). Subsequently, 100 µL of CCK8 solution was introduced into each well, and the plates were incubated for an additional 2-hour period. Finally, the optical density (OD) at a wavelength of 450 nm was determined using a microplate reader (BioTek #Synergy LX, VT, USA). The relative cell viability (or proliferation rate) = (value of the experimental group ÷ value of the control group) × 100%.

Live-Dead Staining

The cytotoxicity of exosomes was evaluated *in vitro* via live-dead staining (Beyotime #C2015S, Shanghai, China). To balance experimental efficiency and result reliability, the sample size (n) was set to 7 in this experiment. HUVECs were plated at 1×10^4 cells per well in 24-well plates and allowed to adhere for 12 h. Then, Exos and RBP3-Exos, suspended in DMEM to 50 µg/mL, were introduced to the cultures and maintained for 48 h under hypoxic conditions (1% O_2). Cells from the same batch as the experimental group were treated with absolute ethanol for 20 minutes prior to staining to induce cell death, which served as the positive control. After that, cells were subjected to staining with calcein-AM, identifying viable cells, and propidium iodide, marking deceased or late-stage apoptotic cells, for a duration of 20 min. Fluorescence imaging was then conducted using microscopy. The results of live/dead staining were statistically analyzed and compared using the ratio of the number of dead cells to the total number of cells (live cells plus dead cells).

RNA Sequencing (RNA-seq)

Under hypoxic conditions (1% oxygen), Exos or RBP3-Exos at a concentration of 1.5 mg/mL were added to the culture medium, adjusted to a final concentration of 50 µg/mL, and incubated for 48 hours. RNA extraction was performed using the RNA Easy Fast Tissue/Cell Kit (Tiangen #DP451, Shanghai, China). Pathway enrichment analysis was investigated utilizing the KEGG (http://www.genome.jp/kegg/) and GO (http://geneontology.org/) databases. For DEG analysis, we obtained the gene expression matrix via transcriptome sequencing, filtered significant DEGs by normalization (FPKM) and statistical tests (DESeq2, $|\log2FC| \geq 1$, adjusted $p < 0.05$). KEGG enrichment showed DNA replication as one of the most enriched pathways (smallest adjusted *p*, highest gene proportion). We then focused on its downregulated DEGs, sorted by differential significance (larger $|\log2FC|$, smaller adjusted *p*), and selected core downregulated factors with clear functional relevance as target genes (*LIG1*, *POLD1*, *MCM7*, *MCM6*, *POLE2*, *MCM3*). Subsequent molecular experiments will verify their roles. This strategy ensures biological relevance and statistical significance, providing reliable candidates for mechanism research.

Flow Cytometry Cell Cycle Analysis

Logarithmically growing vascular endothelial cells were collected, digested, and centrifuged; the supernatant was discarded to obtain cell pellets. Pre-cooled PBS was added to the pellets to resuspend the cells, followed by another centrifugation to discard the supernatant for thorough washing. Subsequently, 1 mL of pre-cooled 70% ethanol was added, and the cells were gently pipetted to disperse uniformly before being fixed at 4 °C overnight. The next day, the fixed cells were collected by centrifugation and washed twice with PBS to completely remove ethanol residues. According to the instructions of the Cell Cycle Detection Kit (Beyotime #C1052, Shanghai, China), a staining working solution was prepared by adding 25 µL of PI staining solution and 10 µL of RNase A to 500 µL of buffer. The working solution was added to the cell pellets for resuspension, and the cells were incubated at 37 °C in the dark for 30 minutes. After staining, the cell suspension was filtered through a 300-mesh nylon mesh to remove aggregated impurities, and detected using a flow cytometer (Sony #Cell Sorter SH800S, Tokyo, Japan) with an excitation wavelength set at 488 nm to collect red fluorescence signals. FlowJo software (10.8.1, Becton, Dickinson and Company, Palo Alto, CA, USA) was used to analyze the cell cycle distribution and calculate the proportions of cells in G1, S, and G2 phases. The experiment was independently repeated three times to ensure the reliability of the results.

Real-Time Quantitative PCR (qPCR)

cDNA synthesis was executed with an RNA reverse transcription kit (Yeason #11141ES, Shanghai, China) as prescribed, with the resulting product stored at –80 °C. The internal reference gene Actin was employed for the quantification of LIG1, POLD1, MCM7, MCM6, POLE2 and MCM3 transcripts (**Supplementary Table 1**). Relative quantification of gene expression was conducted using Power SYBR Green PCR Master Mix (Yeason #11184ES, Shanghai, China) following the qRT-PCR mixture's specified protocol. The qPCR instrument used is QuantStudio 3. For its quantitative calculation method, each gene corresponds to 10 µL of SYBR, 0.4 µL of forward primer (F), and 0.4 µL of reverse primer (R); each sample corresponds to 7.2 µL of DEPC water and 2 µL of cDNA. Each sample underwent triplicate amplification runs, and the mean value from these was defined as a single biological replicate. The results were statistically analyzed using the $2^{-\Delta\Delta Ct}$ method.

Western Blotting

Cellular protein were isolated from HUVECs using RIPA lysis buffer supplemented with both phosphatase (Sharebio #SB-WB017, Shanghai, China) and protease inhibitors (Sharebio #SB-WB016, Shanghai, China), each at a 1% concentration. Quantification of protein level was conducted via a BCA assay (Servicebio #G2026, Wuhan, China). Following preparation in 5× SDS-PAGE loading buffer (Epizyme #LT101, Shanghai, China) and heat denaturation, the samples underwent electrophoretic separation on 10% gels (Epizyme #PG004, Shanghai, China) and were subsequently transferred onto PVDF membranes (Millipore #ISEQ00010, Billerica, MA, USA). The membranes, after a blocking step, received an overnight incubation with primary antibodies (**Supplementary Table 2**), followed by exposure to HRP-conjugated secondary anti-

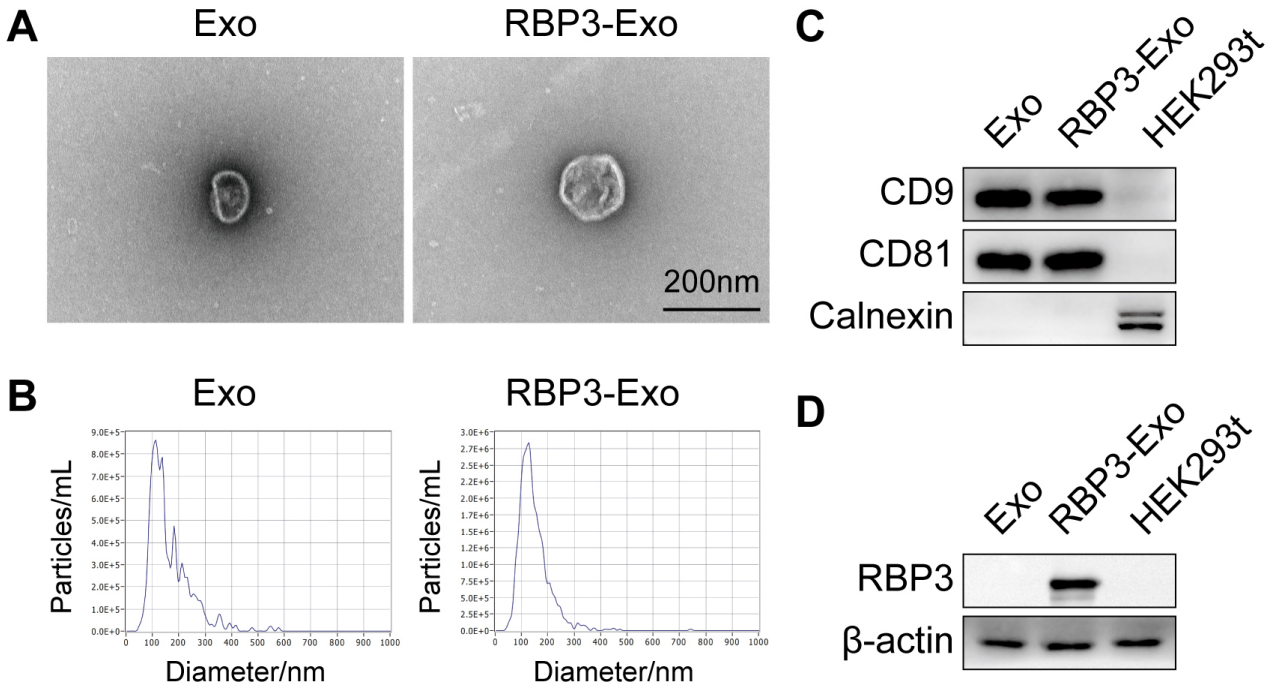

Fig. 1. Characterization of Exo and RBP3-Exo. (A) Representative TEM illustrating the morphology of isolated Exo and RBP3-Exo. Scale bars: 200 nm. (B) NTA was utilized to determine the size distribution profiles for both exosome groups. (C) Immunoblotting analysis confirmed the presence of exosomal markers CD9 and CD81 in Exo and RBP3-Exo preparations, while also detecting Calnexin expression in HEK293t cell lysates. (D) Protein expression of RBP3 was verified through Western blot in Exo, RBP3-Exo and HEK293t cells. Exo, exosomes; RBP3, retinol-binding protein 3; TEM, transmission electron microscopy; NTA, nanoparticle tracking analysis.

bodies (**Supplementary Table 2**). Signal visualization was achieved with an ECL system, and band intensity was quantified employing ImageJ software.

Mice

The mice were purchased from Leagene Biotechnology, and they were of the C57BL/6 strain, including 50 two-day-old pups and 2 mother mice. For the OIR model, approximately 20 mice were used for model establishment. In the formal experiment, around 10 mice were included in each group. The mice were housed under a 12-hour cyclic light-dark regimen at room temperature (RT). Simple randomization was used for grouping OIR model mice. P12 mice were assigned to Control, Exo, and RBP3-Exo groups (n = 10/group) via Excel-generated random numbers and sorting. Post-grouping statistical verification showed no significant difference in mean body weight among groups ($p > 0.05$) (**Supplementary Table 3**). In the Exo group and RBP3-Exo group, 1 µL of exosomes (with a concentration of approximately 1.5 mg/mL determined by the BCA method) were injected into each eye, at the posterior side of the limbus corneae of mice. The body weight of the mice at P17 was about 5–6 g. Anesthesia was performed using 3% sodium pentobarbital at a dose of 60 mg/kg, and the mice were euthanized immediately after anesthesia via cervical dislocation. All surgical procedures were performed following anesthesia induced by sodium pentobarbital, with utmost efforts dedicated to the alleviation of animal distress. The execution of all *in vivo* experiments adhered strictly to the NIH Guide for the Care and Use of Laboratory Animals and received formal approval from the Institutional Animal Care and Use Committee at Shanghai Changhai Hospital (CHEC (A.E)2025-052).

Oxygen-Induced Retinopathy (OIR)

The OIR model was established according to our previously documented protocol [21,22,32]. Ambient oxygen concentration was constantly tracked employing an oxygen analyzer (XBS-03S, HangZhou Aipu Instrument Equipment, Hangzhou, China). The OIR model is susceptible to subtle variations in experimental conditions (e.g., oxygen concentration during hypoxia induction, mouse age at model establishment), leading to significant inter-individual variability in pathological indicators. A larger sample size is required to reduce random errors; thus, the sample size (n) was set to 10 in this experiment. Induction involved housing C57BL/6J neonatal mice with their dam in a high-oxygen environment (75 ± 0.5%) from postnatal day 7 to 12. Upon return to normoxia on P12, pups were randomly allocated into three cohorts receiving intravitreal injections of either PBS, Exos or RBP3-Exos (resuspended in PBS). Euthanasia was performed on P17, fol-

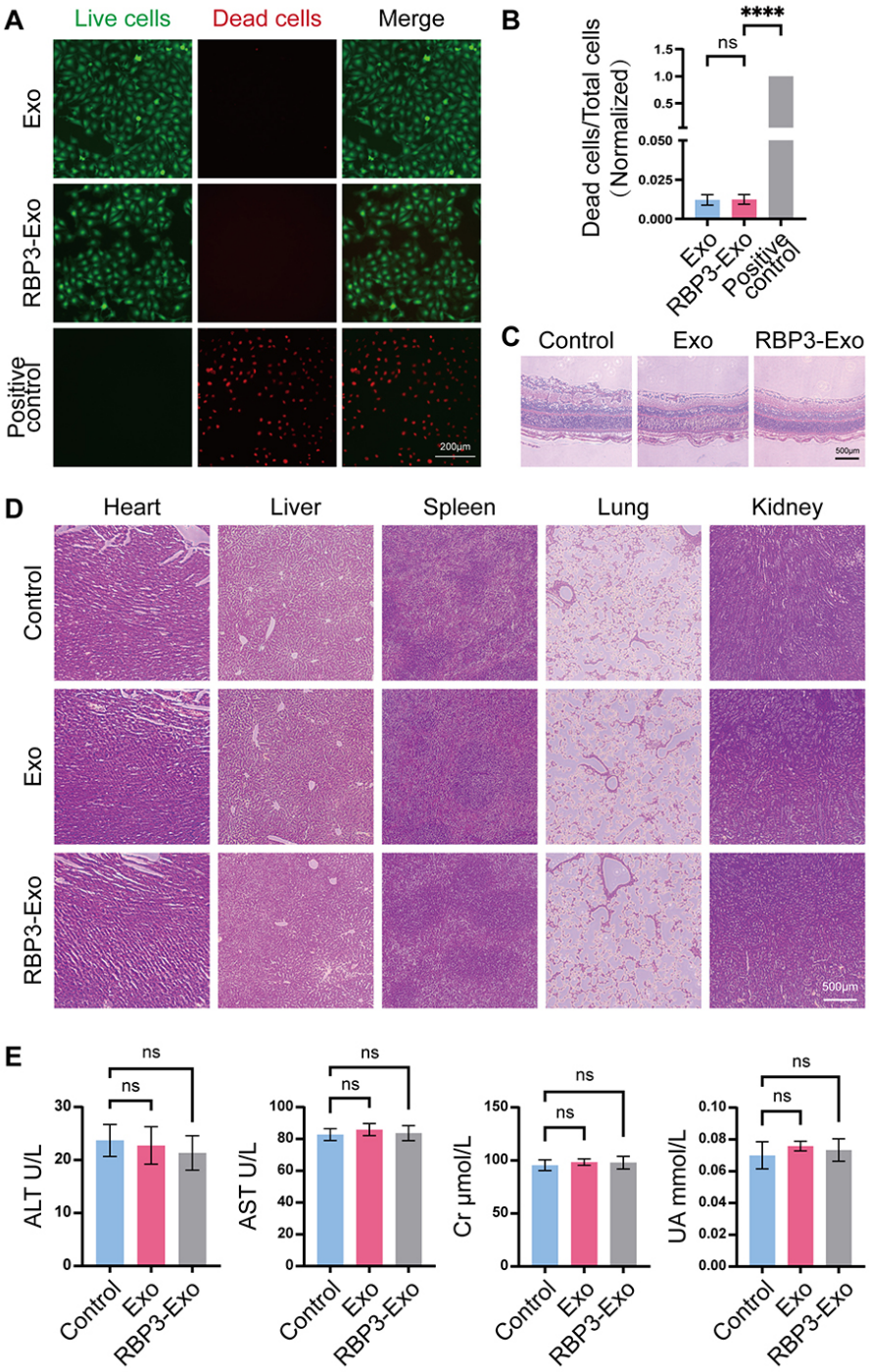

Fig. 2. Toxicity of Exo and RBP3-Exo. (A) Fluorescence microscopy depicting HUVECs after exposed to Exo and RBP3-Exo under hypoxic condition for 48 h. Scale bars: 200 μm. Cellular viability was assessed via Calcein AM (green, live cells) and Propidium Iodide (red, dead cells) staining. (B) Quantification of cell viability from the live-dead assay. Data were presented as means ± SE, n = 7, one-way ANOVA, Dunnett *t* test; ns means no significance, ****$p < 0.0001$. (C) HE-stained retinal tissue from P17 mice under varying treatments. Tissues were examined from n = 3 mice per experimental cohort. Scale bar: 500 μm. (D) Histological assessment by HE staining of major organs, including the heart, liver, spleen, lung, liver and kidney. Scale bar: 500 μm. (E) Hepatic and renal function of the blood from mice after treatment with PBS, Exo or RBP3-Exo. The data are presented as the means ± SE. n = 6, two-tailed *t*-test. ns means no significance. ANOVA, Analysis of Variance; HE, Hematoxylin-Eosin.

lowed by eye enucleation for subsequent immunofluorescence assays. Avascular area is defined as the area in retinal flat mounts with no IB4-positive signal. The boundary was manually outlined using ImageJ (1.54f, National Institutes of Health, USA) to calculate the area, and the result was expressed as "the percentage of avascular area to the total retinal area". Neovascular area is defined as IB4-positive clustered abnormal vascular tufts. The result was quantified as "the percentage of the total area of neoangiogenic tufts to the total retinal area".

Retina Immunofluorescence

Following enucleation, eyes were immersed in 4% PFA (Servicebio #G1101, Wuhan, China) for 1 h of fixation. Subsequent blocking was performed using a solution of 5% BSA (Yeason #36101ES60, Shanghai, China) and 0.05% Triton-X-100 (Servicebio #GC204003, Wuhan, China), supplemented with PBS, after which retinal samples underwent overnight incubation at 4 °C with IB4 (Vector #FL-1201). Application of Apollo fluorescent azide proceeded for 30 min at RT, prior to final mounting. We performed imaging using fluorescence microscopy and confocal microscopy, and finally analyzed the quantification of non-perfusion areas, quantification of neovascular tufts, and the colocalization relationship between neovascularization and proliferating cells using ImageJ software (1.54f, National Institutes of Health, USA), respectively. Images were acquired using a fluorescence microscope (Biotek #Cytation 5, VT, USA). The excitation wavelength of IB4 was set to 488 nm, and the emission wavelength to 525 nm. Images were captured with a 4× objective to obtain the overall field of view of the retinal vascular network, clearly showing the overall distribution of retinal blood vessels. Images were acquired using a laser confocal scanning microscope (Zeiss #LSM 880, Oberkochen, Baden-Württemberg, Germany). The excitation wavelength was 488 nm, and the emission wavelength was 525 nm. Z-stack scanning was performed with a high-magnification 20× objective at a step size of 3 µm to obtain three-dimensional spatial information of the vascular structure. Finally, the Z-stack data were reconstructed into a two-dimensional image through maximum intensity projection (MIP), clearly presenting the fine structure and spatial distribution characteristics of blood vessels.

Hematoxylin-Eosin (HE) and Blood Biochemistry Analysis

For assessment of RBP3-Exos' biological safety, vital organs (eyes, heart, liver, spleen, lungs, and kidneys) were harvested from mice following intravitreally injection and fixed in 4% PFA (Servicebio #G1101, Wuhan, China). Subsequent processing involved paraffin embedding, sectioning at 8 µm thickness, and HE staining (JKchem #71014460, Shanghai, China). To evaluate the potential hepatotoxicity and nephrotoxicity of RBP3-Exo, the researchers performed several blood biochemical tests, including alanine transaminase (ALT, Rayto #R01502, Shenzhen, China), aspartate transaminase (AST, Rayto #R01702, Shenzhen, China), creatinine (Cr, Rayto #R05602, Shenzhen, China), and uric acid (UA, Rayto #R03102, Shenzhen, China), using an automatic biochemical analyzer (Rayto #Chemray 240, Shenzhen, China).

Statistical Analysis

All statistical evaluations were conducted using GraphPad Prism (GraphPad software 10.0, Sandiego, CA, USA). Inter-group comparisons utilized independent sample t tests, while assessments involving more than two groups employed Analysis of Variance (ANOVA). For one-way analysis of variance, Dunnett's test was used for post-hoc testing. Experimental procedures were executed in triplicate, and p values < 0.05 were considered as statistically significant ($^{*}p < 0.05$; $^{**}p < 0.01$; $^{***}p < 0.001$; $^{****}p < 0.0001$).

Result

Characterization of RBP3-Exos

The isolation of Exos and RBP3-Exos from cell culture supernatants was achieved through standard differential centrifugation. Their characterization involved TEM, NTA, and Western blotting (Fig. 1A–C). TEM showed that both types of exosomes exhibited a cup-shaped morphology. NTA revealed that the average sizes of Exos and RBP3-Exos were 136.8 nm and 131.5 nm, respectively. The exosome-specific markers CD9 and CD81 were detected in both types of exosomes, while Calnexin expression was not detected, indicating that the isolated vesicles were exosomes rather than cells. We confirmed that the exosomes (RBP3-Exo) secreted by HEK293t cells transfected with the RBP3 plasmid contain the RBP3 protein via Western blot (Fig. 1D).

We further assessed the biosafety profile of RBP3-Exos both *in vitro* and *in vivo*. For the *in vitro* assay, live-dead staining was conducted utilizing Calcein to identify viable cells and propidium iodide (PI) to mark dead cells. The results indicated that RBP3-Exos were non-toxic to HUVECs ($p < 0.0001$) (Fig. 2A,B). *In vivo*, HE staining of major organs (retina, heart, liver, spleen, lung, kidney) was conducted at the endpoint of the OIR model, revealing no toxic effects on vital tissues following intravitreal injection of RBP3-Exos resuspended in PBS (Fig. 2C,D). Further blood biochemical and routine examinations confirmed the safety of RBP3-Exos. These parameters displayed no notable alterations, indicating minimal systemic toxicity associated with RBP3-Exos (Fig. 2E, **Supplementary Table 4**).

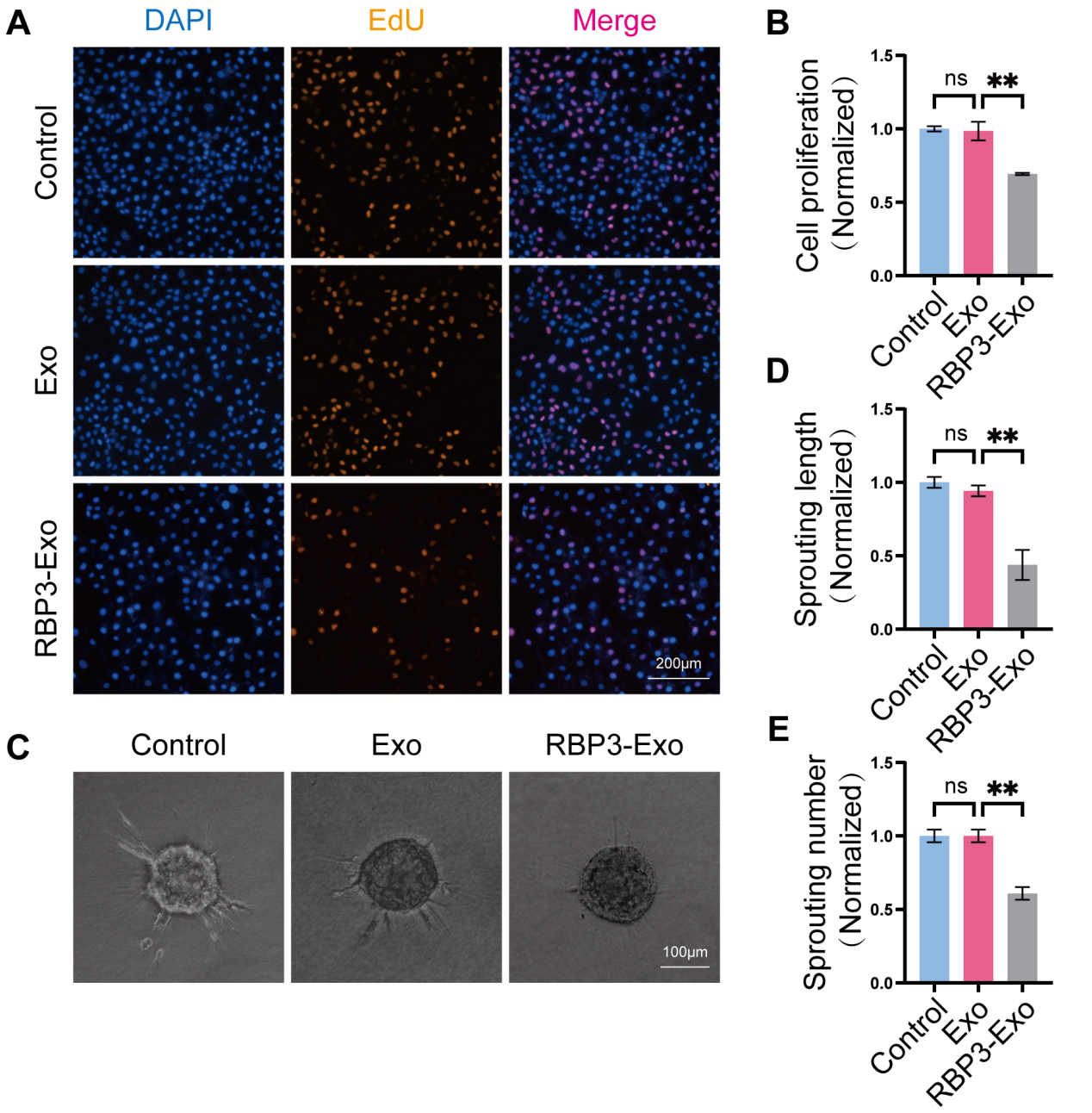

Fig. 3. RBP3-Exo inhibits angiogenesis *in vitro*. Shown are representative images (A) and quantification (B) from EdU performed on HUVECs cultured with PBS, Exo or RBP3-Exo under hypoxic condition for 48 h. Cells positive for EdU (yellow) and DAPI (blue) indicate proliferating and total cell populations, respectively. Scale bar: 200 μm. Also displayed are representative images (C) and quantification (D,E) from sprouting assay using HUVECs treated with Exo or RBP3-Exo under hypoxic condition for 24 h. Scale bar: 100 μm. Data were presented as means ± SE, n = 3, one-way ANOVA, Dunnett *t* test; ns means no significance, $^{**}p < 0.01$. EdU, 5-ethynyl-2′-deoxyuridine; DAPI, 4′,6-Diamidino-2-phenylindole dihydrochloride.

RBP3-Exo Inhibits Angiogenesis In Vitro

DiD fluorescent labeling was applied to exosomes, and subsequent uptake by HUVECs was visualized through fluorescence microscope. For cellular staining, HUVECs were treated with F-actin, an established marker for cytoskeleton, alongside DAPI, frequently employed to identify nuclei. Immunofluorescence data demonstrated that both Exos and RBP3-Exos were readily internalized by HUVECs (**Supplementary Fig. 1**).

The CCK-8 assay, which relies on the quantification of metabolically active cells via the formation of a water-soluble formazan dye, was employed to assess cellular vi-

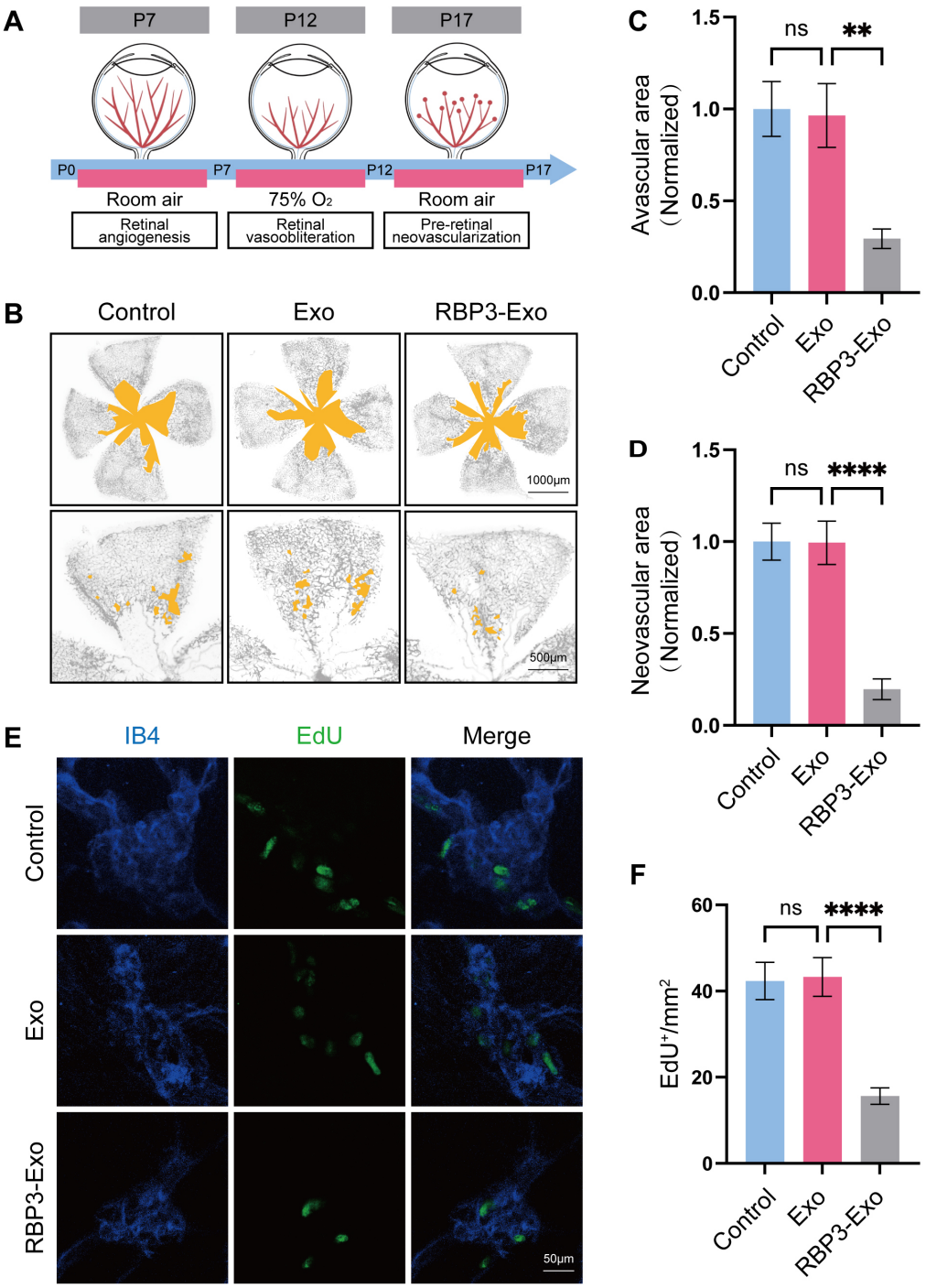

Fig. 4. RBP3-Exo inhibits angiogenesis *in vivo*. (A) Schematic representation of the OIR model and sequential stages of retinal pathology. (B–D) Intravitreal delivery of Exo or RBP3-Exo resuspended in PBS markedly alleviated oxygen-induced retinopathy (B), reflected by decreased avascular area, the area in retinal flat mounts with no IB4-positive signal (C) and diminished neovascular area, IB4-positive clustered abnormal vascular tufts (D). Yellow zones denote central retinal avascular area, alongside visible neovascular tufts. Scale bar: 1000 μm, 500 μm. (E) Immunofluorescence staning of retinal sections from P17 OIR mice. IB4 (blue) and EdU (green) label blood vessel and proliferating cells, respectively. Scale bar: 50 μm. (F) Quantitative analysis of proliferating endothelial cells. Data were presented as means ± SE, n = 10, one-way ANOVA, Dunnett *t* test; ns means no significance, $^{**}p < 0.01$, $^{****}p < 0.0001$. OIR, oxygen-induced retinopathy.

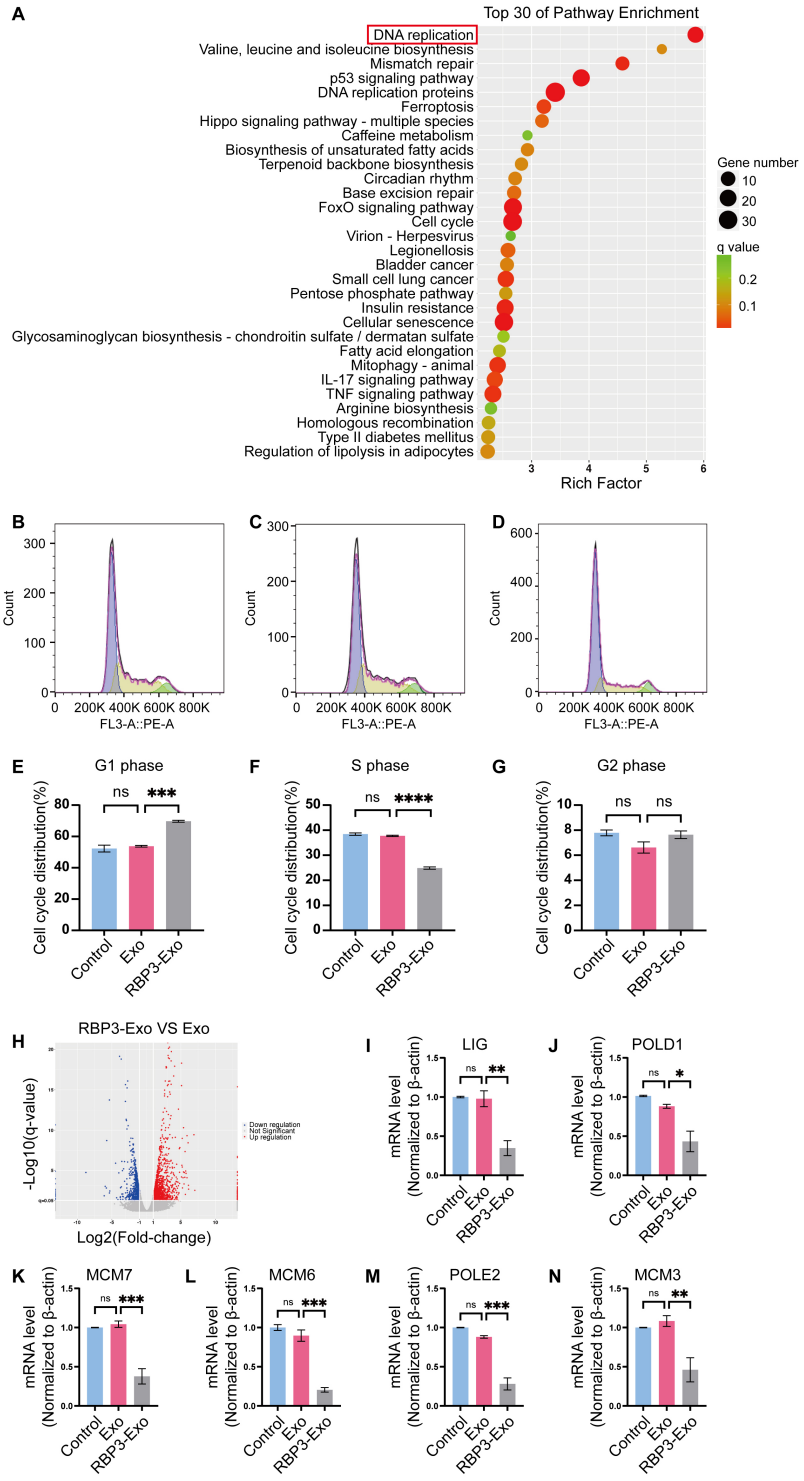

Fig. 5. RBP3-Exo regulates the RNA expression of genes involved in DNA replication. (A) Representative RNA sequence of the top 30 pathway enrichment. The DNA replication pathway in the red frame represents the significantly different pathway we chose for our experiments. (B–D) Flow cytometry detected the distribution of HUVECs cell cycle phase after treated by PBS, Exo or RBP3-Exo under hypoxia condition in 48 h. (E–G) G1, S and G2 phases distribution of HUVEC under different treatments. (H) Volcano plot of Log2 fold-changed genes for Exo or RBP3-Exo treatment. (I–N) The mRNA levels of DNA replication related gene in Exo or RBP3-Exo treated HUVECs under hypoxia condition in 48 h determined by qPCR. n = 3. Data were presented as means ± SE, n = 3, one-way ANOVA, Dunnett *t* test; ns means no significance, *$p < 0.05$, **$p < 0.01$, ***$p < 0.001$, ****$p < 0.0001$. qPCR, quantitative real-time PCR.

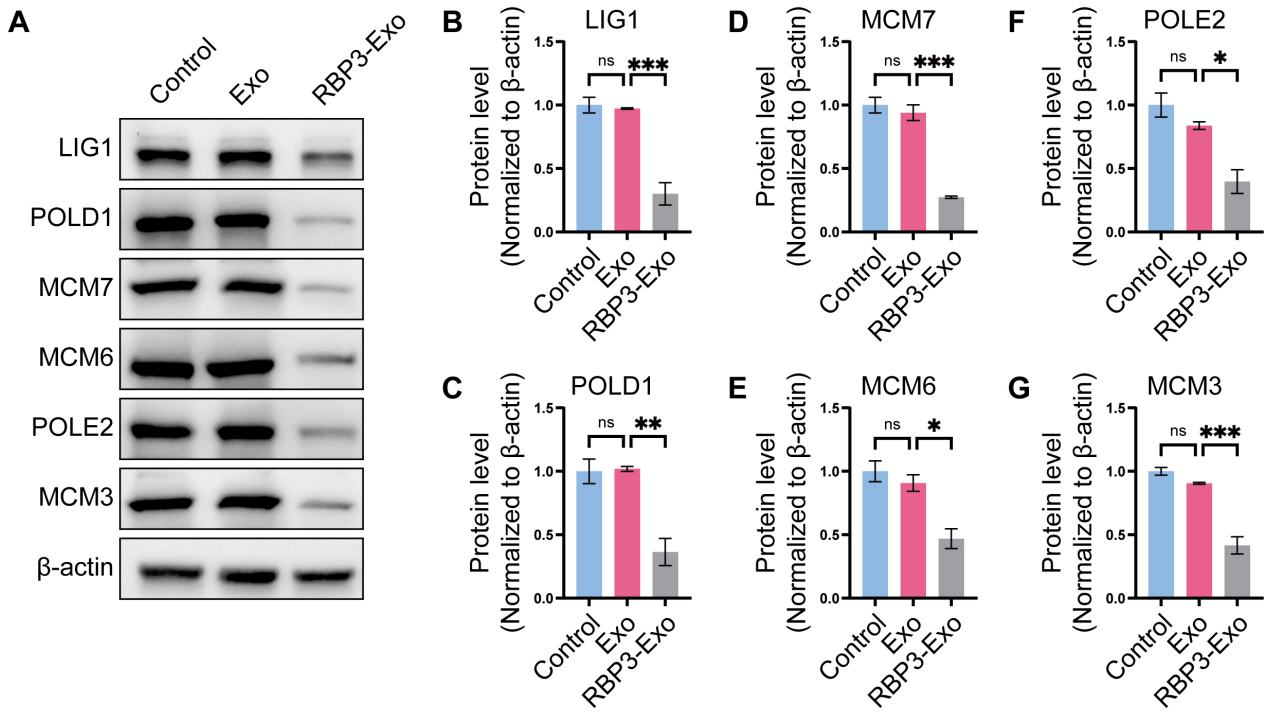

Fig. 6. RBP3-Exo regulates the protein level of genes involved in DNA replication. Representative immunoblots (A) and quantification (B–G) for DNA replication related protein levels in PBS, Exo or RBP3-Exo treated HUVECs in hypoxia environment in 48 h. n = 3. Data were presented as means ± SE, n = 3, one-way ANOVA, Dunnett *t* test; ns means no significance, *$p < 0.05$, **$p < 0.01$, ***$p < 0.001$.

ability and proliferation. Following a 48-hour incubation period with either Exos or RBP3-Exos, absorbance measurements at 450 nm revealed that RBP3-Exos significantly suppressed cellular activity when compared to the Exos treatment group ($p < 0.0001$) (**Supplementary Fig. 2**).

The influence of RBP3-Exos on HUVECs proliferation was assessed via the 5-ethynyl-2′-deoxyuridine (EdU) incorporation assay. EdU is widely employed to assess cell proliferation. Statistical analysis showed no significant difference between the Exo group and the Control group, while a significant difference was observed between the RBP3-Exo group and the Exo group ($p < 0.01$). The results suggested that RBP3-Exos significantly inhibited HUVECs growth compared to Exos (Fig. 3A,B).

Angiogenic potential of vascular endothelial cells was examined using a spheroid-sprouting assay, a model capturing proliferative and migratory behavior in three-dimensional settings. Results indicate that RBP3-Exos suppressed both sprout length ($p < 0.01$) and number ($p < 0.01$) of HUVECs (Fig. 3C–E).

These results indicate that RBP3-Exos exhibit biocompatibility and demonstrate promising anti-angiogenic capacity *in vitro*.

RBP3-Exo Inhibits Angiogenesis In Vivo

The OIR mouse model effectively mirrors the pathological development of human ROP (Fig. 4A). Findings from this model revealed that intravitreal administration of RBP3-Exos resuspended in PBS led to a marked reduction in both avascular ($p < 0.01$) and neovascular ($p < 0.0001$) regions, decreasing 70% and 80% respectively, showing a clear divergence from PBS-treated controls (Fig. 4B–D). Given that proliferating endothelial cells drive the emergence of neovascular tufts, we detected the proportion of proliferating cells (via EdU staining) within neovascular clusters (via IB4 staining) using fluorescent staining. Our results further demonstrate the capacity of RBP3-Exos to inhibit endothelial cell proliferation ($p < 0.0001$) (Fig. 4E,F).

Underlying Mechanisms In Vitro

To investigate the function of RBP3-Exos in angiogenesis, qPCR and Western blot were applied to analyses to evaluate their anti-angiogenic properties.

To further elucidate the potential mechanisms by which RBP3-Exos inhibit angiogenesis, RNA-seq was performed. KEGG pathway analysis revealed significant enrichment of these DEGs in DNA replication-related pathways (Fig. 5A). Analysis of cell cycle phase distribution by flow cytometry with PI staining revealed that, com-

pared with the Control group and Exo group, the RBP3-Exo group showed an increase in G1 phase cells ($p < 0.001$) and a decrease in S phase cells ($p < 0.0001$), presenting G1 phase arrest and shortened S phase, which is consistent with the characteristic of impaired DNA replication pathway (Fig. 5B–G).

After administration of RBP3-Exos, 2047 differentially expressed genes (DEGs) were detected, comprising 1301 upregulated and 746 that were downregulated (Fig. 5H). Within this pathway, the most prominently downregulated genes were *LIG1*, *POLD1*, *MCM7*, *MCM6*, *POLE2*, and *MCM3*.

Using Quantitative Real-time PCR, reduced expression of LIG1, POLD1, MCM7, MCM6, POLE2, and MCM3 was confirmed at the transcriptional level after RBP3-Exos intervention (Fig. 5I–N). Protein levels were additionally examined via Western blot analysis. Consistent with the qPCR results, RBP3-Exos significantly suppressed the protein expression of LIG1, POLD1, MCM7, MCM6, POLE2, and MCM3 (Fig. 6A–G).

RBP3-Exos may exert protective effects through multiple mechanisms. Existing literature indicates that RBP3 suppresses pTyr-VEGFR2, potentially via interfering with VEGF-VEGFR2 [15]. Our findings corroborate this observation. Data from qPCR and Western Blot analyses demonstrated that administration of RBP3-Exos downregulated VEGF-associated RNA ($p < 0.01$) and protein levels ($p < 0.05$) (**Supplementary Fig. 3A–C**). DNA replication is the basis of cell proliferation, and VEGF promotes proliferation-dependent angiogenesis. In hypoxic TNBC cells, ATR inhibitors targeting DNA replication sites significantly inhibited the hypoxia-induced increase in VEGFA expression [33].

Discussion

In the field of treating pathological retinal neovascular diseases, engineered extracellular vesicles (EVs) exhibit prominent therapeutic potential due to their biocompatibility advantages [31]. To construct a therapeutic carrier for diabetic retinopathy, we transfected plasmids carrying the RBP3 gene into HEK293t cells via transfection technology. Leveraging the cells' inherent secretion mechanism, we successfully prepared engineered EVs loaded with RBP3 protein. Subsequent experiments showed that there were no significant differences in core physical properties between these engineered EVs and unmodified EVs through TEM and NTA. This confirms that genetic modification did not affect their basic structure and function.

Through viability staining, HE staining, and blood biochemical tests, this study found no significant differences between the RBP3-Exo group and the Exo group, indicating that RBP3-Exo has good biosafety. This result is consistent with the conclusion reported by You *et al.* [34] that "genetically modified exosomes do not alter their basic safety", suggesting that the introduction of the *RBP3* gene does not introduce additional toxic risks. The reason may be that when HEK293t cells secrete exosomes, they only target and integrate the RBP3 protein into the exosome membrane or interior without changing the core structure and biocompatibility of exosomes. However, this study has certain limitations: the OIR model was used only for short-term safety evaluation, and the tissue accumulation effect after long-term administration was not involved; in addition, blood biochemical tests only covered liver and kidney function indicators, not immune-related parameters such as inflammatory factors. Subsequent studies need to supplement these aspects to improve the safety evidence.

This study confirmed the biocompatibility and anti-angiogenic capacity of RBP3-Exo through multi-dimensional experiments, providing key evidence for its treatment of pathological retinal neovascularization. In terms of biocompatibility, exosome uptake experiments verified that RBP3-Exo exerts effects from within cells, combined with previous viability staining, HE staining, and blood biochemical results, it is confirmed that RBP3-Exo has good biosafety. Regarding anti-angiogenic function, CCK8 assay, EdU assay and Sprouting assay confirm that it blocks angiogenesis at multiple links including proliferation and sprouting, which is presumably related to the regulation of pathways such as VEGF/VEGFR, and the specific molecular mechanisms are further verified in the latter part of the study. This study still has certain limitations: it failed to clarify the specific intracellular targets of RBP3 protein (such as lysosomes, endoplasmic reticulum, etc.) through fluorescence staining. Subsequent studies can focus on the above directions and supplement exosome tracing experiments to improve the mechanism of action and therapeutic evidence chain of RBP3-Exo.

This study provided *in vivo* experimental evidence for the anti-neovascularization effect of RBP3-Exo through fluorescence staining-based analysis of key indicators in the retinas of OIR model mice, which is consistent with the conclusion from *in vitro* CCK8, EdU, and Sprouting experiments that "RBP3-Exo inhibits endothelial cell proliferation and migration". Further analysis of the proportion of proliferating cells in neovascular tufts suggests that the core mechanism of RBP3-Exo's anti-angiogenic effect may be achieved by inhibiting the proliferative activity of endothelial cells within neovascular tufts, rather than simply destroying the already formed vascular structure.

Based solely on previous safety data, this study evaluated a single intravitreal administration dose of the test exosome. Due to the lack of dose-response data with multiple gradient doses, it was impossible to determine the optimal therapeutic window required for clinical use (including the minimum effective dose and maximum tolerated dose), which hinders the translation of results to clinical practice—clinical settings often require individualized dose adjustments. In the future, dose-response relationships will be

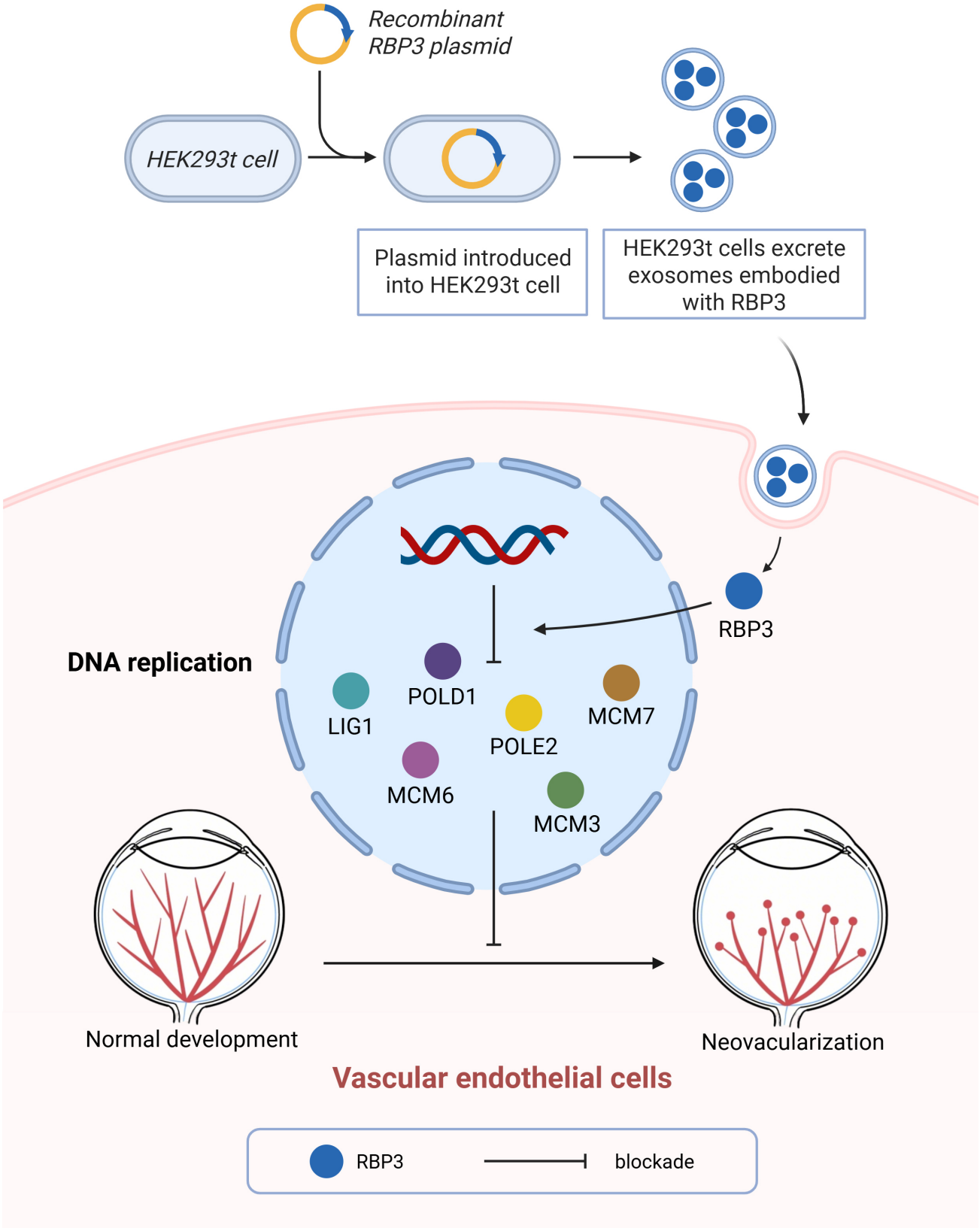

Fig. 7. Illustration showing the expression pattern and role of RBP3-Exo during retinal neovascularization (RNV). Created with BioRender (https://www.biorender.com).

explored through multi-concentration gradient tests combined with long-term safety monitoring (such as optical coherence tomography for retinal structure and inflammation detection). We now clarify that our findings provide preliminary preclinical evidence for the potential therapeutic value of the test agent/exosomes in retinal diseases, rather than direct clinical applicability.

Additionally, this study only measured the preparation concentration of exosomes and initially observed their retinal localization through fluorescence imaging, but did not quantitatively analyze their biodistribution dynamics and half-life in retinal tissues (such as the ganglion cell layer, inner/outer nuclear layers), which is crucial for understanding the treatment duration and target cell specificity. Subsequent studies will fill this gap using tissue separation combined with quantitative PCR or radiolabeling technology.

This study initially revealed the molecular mechanism by which RBP3-Exo inhibits angiogenesis through RNA-seq combined with flow cytometry, qPCR and WB experiments, providing key evidence for its targets (Fig. 7). In current research on the treatment of neovascular diseases, engineered exosomes mostly exert effects by delivering miRNAs to regulate inflammation or classical angiogenesis pathways. For example, exosomes delivering miR-205 block pathological neovascularization and vascular leakage by dual-target inhibition of VEGFA and ANGPT2; hypoxic preconditioning enhances the therapeutic efficacy of M2 macrophage-derived exosomes (Hypo-Exos), which regulate chondrocyte function through the miR-124-3p/STAT3 axis to alleviate knee osteoarthritis (KOA) degeneration [26,35]. In addition, most anti-angiogenic studies focus on classical pathways such as VEGF/VEGFR, blocking angiogenesis by inhibiting receptor binding or downstream MAPK and PI3K-Akt signaling [6,7,10].

In contrast, the core new finding of this study is that RNA-seq differential analysis showed that after RBP3-Exo treatment, the most significantly differentially regulated pathway in vascular endothelial cells is the DNA replication pathway, among which genes such as *LIG1*, *POLD1*, *MCM7*, *MCM6*, *POLE2*, and *MCM3* are the most downregulated. These genes are all core regulators of the DNA replication process: MCM family proteins are key components of DNA helicase responsible for initiating DNA replication; POLD1 and POLE2 are DNA polymerase subtypes involved in DNA strand synthesis; LIG1 regulates DNA strand ligation, and these genes collectively maintain the orderly progress of DNA replication [36–40].

It should be noted that this study has not clarified how the RBP3 protein specifically regulates these DNA replication-related genes (e.g., whether by directly binding to gene promoters or regulating upstream transcription factors), nor has it explored whether the downregulation of these genes affects other pathways. In the future, ChIP-seq, dual-luciferase reporter gene experiments, etc., can be used to further explore the regulatory relationship between RBP3 and target genes and improve the mechanism chain. Meanwhile, the *in vivo* experiments of this study were based on a mouse model (OIR model), and the observed effects on DNA replication and retinal vascular regeneration are mouse-specific. There are species differences in DNA replication-related pathways between mice and human, which may lead to inconsistent efficacy in clinical applications. In the future, human retinal pigment epithelial cells or retinal organoids will be used to verify the regulation of human DNA replication pathways by RBP3-Exo, reducing the impact of species differences.

Conclusion

This study, through *in vitro* cellular functional assays and *in vivo* mouse OIR models, confirms that RBP3-Exos attenuate DNA replication function under hypoxic conditions, thereby ameliorating retinal neovascularization and playing a critical role in preventing the progression of severe DR. By combining multi-omics and molecular experiments, this study clarified the molecular mechanism by which RBP3-Exo inhibits angiogenesis. It confirmed that RBP3-Exo can downregulate the expression of key genes in the DNA replication pathway (such as LIG1, POLD1, and the MCM family), block the DNA replication process of vascular endothelial cells, and ultimately inhibit cell proliferation and angiogenesis. In summary, this investigation establishes that RBP3-Exos are instrumental in modulating pathological retinal angiogenesis. These exosomes significantly suppress neovascularization both *in vivo* and *in vitro*. Relative to conventional anti-VEGF treatments, this approach may diminish systemic immune reactions and lower resistance risks, positioning it as a compelling therapeutic candidate for retinal vascular diseases that warrants additional study.

Availability of Data and Materials

The data underpinning the plots presented in this paper, as well as other findings from this study, are accessible through the corresponding author upon reasonable request.

Author Contributions

HMZ and MZ designed the research study; WZ, MZW, YXL, HZ and MP performed the research; ZN, JJJ, CYD and XWW collected and analyzed the data; HYS and WS made substantial contributions to conception. HYS and WS have been involved in drafting the manuscript and all authors have been involved in revising it critically for important intellectual content. All authors gave final approval of the version to be published. All authors have participated sufficiently in the work to take public responsibility for appropriate portions of the content and agreed to be accountable for all aspects of the work in ensuring that questions related to its accuracy or integrity.

Ethics Approval and Consent to Participate

All animal experiments were approved by the Institutional Animal Care and Use Committee of Shanghai Changhai Hospital (CHEC (A.E)2025-052).

Acknowledgment

Thanks to Dan Shi (State Key Laboratory of Genetic Engineering, Fudan University, Shanghai, China) for providing technical assistance.

Funding

This study was funded by National Natural Science Foundation of China (82271106, 82171081), 234 Mountain Climbing Plan of Changhai Hospital (No. 2020YXK058).

Conflict of Interest

The authors declare no conflict of interest. Hongyuan Song is serving as one of the Editorial Board members of this journal. We declare that Hongyuan Song had no involvement in the peer review of this article and has no access to information regarding its peer review.

Supplementary Material

Supplementary material associated with this article can be found, in the online version, at https://doi.org/10.24976/Discov.Med.202638204.13.

References

[1] Perais J, Agarwal R, Evans JR, Loveman E, Colquitt JL, Owens D, *et al*. Prognostic factors for the development and progression of proliferative diabetic retinopathy in people with diabetic retinopathy. The Cochrane Database of Systematic Reviews. 2023; 2023: CD013775. https://doi.org/10.1002/14651858.CD013775.pub2.

[2] Eelen G, Treps L, Li X, Carmeliet P. Basic and Therapeutic Aspects of Angiogenesis Updated. Circulation Research. 2020; 127: 310–329. https://doi.org/10.1161/CIRCRESAHA.120.316851.

[3] Wright WS, Eshaq RS, Lee M, Kaur G, Harris NR. Retinal physiology and circulation: effect of diabetes. Comprehensive Physiology. 2020; 10: 933–974. https://doi.org/10.1002/j.2040-4603.2020.tb00135.x.

[4] Zhao F, Hu Z, Li G, Liu M, Huang Q, Ai K, *et al*. Angiogenesis in rheumatoid Arthritis: Pathological characterization, pathogenic mechanisms, and nano-targeted therapeutic strategies. Bioactive Materials. 2025; 50: 603–639. https://doi.org/10.1016/j.bioactmat.2025.04.026.

[5] Levine SR, Sapieha P, Dutta S, Sun JK, Gardner TW. It is time for a moonshot to find "Cures" for diabetic retinal disease. Progress in Retinal and Eye Research. 2022; 90: 101051. https://doi.org/10.1016/j.preteyeres.2022.101051.

[6] Tsai AS, Chou HD, Ling XC, Al-Khaled T, Valikodath N, Cole E, *et al*. Assessment and management of retinopathy of prematurity in the era of anti-vascular endothelial growth factor (VEGF). Progress in Retinal and Eye Research. 2022; 88: 101018. https://doi.org/10.1016/j.preteyeres.2021.101018.

[7] Mettu PS, Allingham MJ, Cousins SW. Incomplete response to Anti-VEGF therapy in neovascular AMD: Exploring disease mechanisms and therapeutic opportunities. Progress in Retinal and Eye Research. 2021; 82: 100906. https://doi.org/10.1016/j.preteyeres.2020.100906.

[8] Zhao X, Seah I, Xue K, Wong W, Tan QSW, Ma X, *et al*. Antiangiogenic Nanomicelles for the Topical Delivery of Aflibercept to Treat Retinal Neovascular Disease. Advanced Materials. 2022; 34: e2108360. https://doi.org/10.1002/adma.202108360.

[9] Tian Y, Zhang F, Qiu Y, Wang S, Li F, Zhao J, *et al*. Reduction of choroidal neovascularization via cleavable VEGF antibodies conjugated to exosomes derived from regulatory T cells. Nature Biomedical Engineering. 2021; 5: 968–982. https://doi.org/10.1038/s41551-021-00764-3.

[10] Campochiaro PA, Akhlaq A. Sustained suppression of VEGF for treatment of retinal/choroidal vascular diseases. Progress in Retinal and Eye Research. 2021; 83: 100921. https://doi.org/10.1016/j.preteyeres.2020.100921.

[11] Chokshi T, Fickweiler W, Jangolla S, Park K, Wu IH, Shah H, *et al*. Reduced Aqueous Retinol-Binding Protein 3 Concentration Is Associated With Diabetic Macular Edema and Progression of Diabetic Retinopathy. Diabetes Care. 2025; 48: 136–142. https://doi.org/10.2337/dc24-1260.

[12] Zeng S, Zhang T, Madigan MC, Fernando N, Aggio-Bruce R, Zhou F, *et al*. Interphotoreceptor Retinoid-Binding Protein (IRBP) in Retinal Health and Disease. Frontiers in Cellular Neuroscience. 2020; 14: 577935. https://doi.org/10.3389/fncel.2020.577935.

[13] Chen J, Shao Y, Sasore T, Moiseyev G, Zhou K, Ma X, *et al*. Interphotoreceptor Retinol-Binding Protein Ameliorates Diabetes-Induced Retinal Dysfunction and Neurodegeneration Through Rhodopsin. Diabetes. 2021; 70: 788–799. https://doi.org/10.2337/db20-0609.

[14] Fickweiler W, Park H, Park K, Mitzner MG, Chokshi T, Boumenna T, *et al*. Elevated Retinol Binding Protein 3 Concentrations Are Associated With Decreased Vitreous Inflammatory Cytokines, VEGF, and Progression of Diabetic Retinopathy. Diabetes Care. 2022; 45: 2159–2162. https://doi.org/10.2337/dc22-0165.

[15] Yokomizo H, Maeda Y, Park K, Clermont AC, Hernandez SL, Fickweiler W, *et al*. Retinol binding protein 3 is increased in the retina of patients with diabetes resistant to diabetic retinopathy. Science Translational Medicine. 2019; 11: eaau6627. https://doi.org/10.1126/scitranslmed.aau6627.

[16] Welsh JA, Goberdhan DC, O'Driscoll L, Buzas EI, Blenkiron C, Bussolati B, *et al*. Minimal information for studies of extracellular vesicles (MISEV2023): From basic to advanced approaches. Journal of Extracellular Vesicles. 2024; 13: e12404. https://doi.org/10.1002/jev2.12404.

[17] Kalluri R, LeBleu VS. The biology, function, and biomedical applications of exosomes. Science. 2020; 367: eaau6977. https://doi.org/10.1126/science.aau6977.

[18] Colombo M, Raposo G, Théry C. Biogenesis, secretion, and intercellular interactions of exosomes and other extracellular vesicles. Annual Review of Cell and Developmental Biology. 2014; 30: 255–289. https://doi.org/10.1146/annurev-cellbio-101512-122326.

[19] Qiu AW, Wang NY, Yin WJ, Zhu ZQ, Liu QH, Zhang WW. Retinal Müller Cell-Released Exosomal MiR-92a-3p Delivers Interleukin-17A Signal by Targeting Notch-1 to Promote Diabetic Retinopathy. Investigative Ophthalmology & Visual Science. 2025; 66: 1. https://doi.org/10.1167/iovs.66.1.1.

[20] Tsai CY, Chen CT, Wu HH, Liao CC, Hua K, Hsu CH, *et al*. Proteomic Profiling of Aqueous Humor Exosomes from Age-related Macular Degeneration Patients. International Journal of

Medical Sciences. 2022; 19: 893–900. https://doi.org/10.7150/ijms.73489.

[21] Song H, Li Q, Gui X, Fang Z, Zhou W, Wang M, *et al*. Endothelial protein C receptor promotes retinal neovascularization through heme catabolism. Nature Communications. 2025; 16: 1603. https://doi.org/10.1038/s41467-025-56810-0.

[22] Gui X, Zhang H, Zhang R, Li Q, Zhu W, Nie Z, *et al*. Exosomes incorporated with black phosphorus quantum dots attenuate retinal angiogenesis via disrupting glucose metabolism. Materials Today Bio. 2023; 19: 100602. https://doi.org/10.1016/j.mtbio.2023.100602.

[23] Wu Y, Li X, Fu X, Huang X, Zhang S, Zhao N, *et al*. Innovative Nanotechnology in Drug Delivery Systems for Advanced Treatment of Posterior Segment Ocular Diseases. Advanced Science. 2024; 11: e2403399. https://doi.org/10.1002/advs.202403399.

[24] Guan J, Meng F, Wang C, Zhang B, Chen J, Han J. Recent advances in engineered exosome-based therapies for ocular vascular disease. Journal of Nanobiotechnology. 2025; 23: 526. https://doi.org/10.1186/s12951-025-03589-3.

[25] Dong X, Lei Y, Yu Z, Wang T, Liu Y, Han G, *et al*. Exosome-mediated delivery of an anti-angiogenic peptide inhibits pathological retinal angiogenesis. Theranostics. 2021; 11: 5107–5126. https://doi.org/10.7150/thno.54755.

[26] Zhang HY, Zhang QY, Liu Q, Feng SG, Ma Y, Wang FS, *et al*. Exosome-loading miR-205: A two-pronged approach to ocular neovascularization therapy. Journal of Nanobiotechnology. 2025; 23: 36. https://doi.org/10.1186/s12951-024-03079-y.

[27] Luo C, Fang C, Zou R, Jiang J, Zhang M, Ge T, *et al*. Hyperglycemia-induced DNA damage response activates DNA-PK complex to promote endothelial ferroptosis in type 2 diabetic cardiomyopathy. Theranostics. 2025; 15: 4507–4525. https://doi.org/10.7150/thno.109514.

[28] Kumar R, Rao GN. Novel role of prereplication complex component cell division cycle 6 in retinal neovascularization. Arteriosclerosis, Thrombosis, and Vascular Biology. 2022; 42: 407–427. https://doi.org/10.1161/ATVBAHA.121.317182.

[29] Hu S, Chen L, Zeng T, Wang W, Yan Y, Qiu K, *et al*. DNA methylation profiling reveals novel pathway implicated in cardiovascular diseases of diabetes. Frontiers in Endocrinology. 2023; 14: 1108126. https://doi.org/10.3389/fendo.2023.1108126.

[30] Hennigs JK, Matuszcak C, Trepel M, Körbelin J. Vascular Endothelial Cells: Heterogeneity and Targeting Approaches. Cells. 2021; 10: 2712. https://doi.org/10.3390/cells10102712.

[31] Zhang H, Mao Y, Nie Z, Li Q, Wang M, Cai C, *et al*. Iron Oxide Nanoparticles Engineered Macrophage-Derived Exosomes for Targeted Pathological Angiogenesis Therapy. ACS Nano. 2024; 18: 7644–7655. https://doi.org/10.1021/acsnano.4c00699.

[32] Zhang H, Cai C, Li Q, Nie Z, Wang M, Liu Y, *et al*. Copper oxide nanoparticles suppress retinal angiogenesis via inducing endothelial cell cuproptosis. Nanomedicine (London, England). 2024; 19: 597–613. https://doi.org/10.2217/nnm-2023-0301.

[33] Barnieh FM, Morais GR, Loadman PM, Falconer RA, El-Khamisy SF. Hypoxia-Responsive Prodrug of ATR Inhibitor, AZD6738, Selectively Eradicates Treatment-Resistant Cancer Cells. Advanced Science. 2024; 11: 2403831. https://doi.org/10.1002/advs.202403831.

[34] You Y, Tian Y, Yang Z, Shi J, Kwak KJ, Tong Y, *et al*. Intradermally delivered mRNA-encapsulating extracellular vesicles for collagen-replacement therapy. Nature Biomedical Engineering. 2023; 7: 887–900. https://doi.org/10.1038/s41551-022-00989-w.

[35] Yu L, Sui B, Fan W, Lei L, Zhou L, Yang L, *et al*. Exosomes derived from osteogenic tumor activate osteoclast differentiation and concurrently inhibit osteogenesis by transferring COL1A1-targeting miRNA-92a-1-5p. Journal of Extracellular Vesicles. 2021; 10: e12056. https://doi.org/10.1002/jev2.12056.

[36] Weissmann F, Greiwe JF, Pühringer T, Eastwood EL, Couves EC, Miller TC, *et al*. MCM double hexamer loading visualized with human proteins. Nature. 2024; 636: 499–508. https://doi.org/10.1038/s41586-024-08263-6.

[37] Gallitto M, Zhang Z. The evolving tale of Pol2 function. Genes & Development. 2023; 37: 72–73. https://doi.org/10.1101/gad.350527.123.

[38] Huang D, Jokela M, Tuusa J, Skog S, Poikonen K, Syväoja JE. E2F mediates induction of the Sp1-controlled promoter of the human DNA polymerase epsilon B-subunit gene POLE2. Nucleic Acids Research. 2001; 29: 2810–2821. https://doi.org/10.1093/nar/29.13.2810.

[39] Jurkiw TJ, Tumbale PP, Schellenberg MJ, Cunningham-Rundles C, Williams RS, O'Brien PJ. LIG1 syndrome mutations remodel a cooperative network of ligand binding interactions to compromise ligation efficiency. Nucleic Acids Research. 2021; 49: 1619–1630. https://doi.org/10.1093/nar/gkaa1297.

[40] Williams JS, Tumbale PP, Arana ME, Rana JA, Williams RS, Kunkel TA. High-fidelity DNA ligation enforces accurate Okazaki fragment maturation during DNA replication. Nature Communications. 2021; 12: 482. https://doi.org/10.1038/s41467-020-20800-1.